

# A solution to the problems of cusps and rotation curves in dark matter halos in the cosmological standard model

A. G. Doroshkevich\*, V. N. Lukash, E. V. Mikheeva

*Astro Space Center of Lebedev Physical Institute, Russian Academy of Sciences, Profsoyuznaya st. 84/32, Moscow, 117997, Russia*

## Abstract

We discuss various aspects of the inner structure formation in virialized dark matter (DM) halos that form as primordial density inhomogeneities evolve in the cosmological standard model. The main focus is on the study of central cusps/cores and of the profiles of DM halo rotation curves, problems that reveal disagreements among the theory, numerical simulations, and observations. A method that was developed by the authors to describe equilibrium DM systems is presented, which allows investigating these complex nonlinear structures analytically and relating density distribution profiles within a halo both to the parameters of the initial small-scale inhomogeneity field and to the nonlinear relaxation characteristics of gravitationally compressed matter. It is shown that cosmological random motions of matter ‘heat up’ the DM particles in collapsing halos, suppressing cusp-like density profiles within developing halos, facilitating the formation of DM cores in galaxies, and providing an explanation for the difference between observed and simulated galactic rotation curves. The analytic conclusions obtained within this approach can be confirmed by the N-body model simulation once improved spatial resolution is achieved for central halo regions.

---

\*Electronic address: [dorr@asc.rssi.ru](mailto:dorr@asc.rssi.ru)

# Contents

<b>1</b>	<b>Indroduction</b>	<b>2</b>
<b>2</b>	<b>The essence and history of the problem</b>	<b>3</b>
<b>3</b>	<b>Dark matter halo</b>	<b>6</b>
<b>4</b>	<b>Entropy of particles in the halo</b>	<b>8</b>
<b>5</b>	<b>Isothermal sphere</b>	<b>9</b>
<b>6</b>	<b>Internal halo structure</b>	<b>14</b>
<b>7</b>	<b>What is needed to form cusps</b>	<b>17</b>
<b>8</b>	<b>Ensemble of protohalos</b>	<b>21</b>
<b>9</b>	<b>From density profile to entropy</b>	<b>23</b>
<b>10</b>	<b>Initial cosmological perturbations</b>	<b>27</b>
<b>11</b>	<b>A solution to the problem of galactic cusps</b>	<b>31</b>
<b>12</b>	<b>Galactic rotation curves</b>	<b>34</b>
<b>13</b>	<b>Effect of the background entropy</b>	<b>37</b>
<b>14</b>	<b>Conclusion</b>	<b>39</b>
<b>15</b>	<b>Appendices</b>	<b>39</b>

## 1 Introduction

This review is the second of two (see [1]) devoted to the formation of the large-scale structure of the Universe and problems of virialized dark matter (DM) halos. We do not attempt to discuss all related problems of the physical cosmology and focus in fact on DM evolution in the cosmological standard model (CSM). The discussion is based on the original papers of the authors and follows the chapters of book [2]. Here, we present a more

detailed discussion of these problems using new observational data and a comparison with the theory without invoking detailed analytic calculations (theoretical results are described in the appendices; see [2] for the proofs).

## 2 The essence and history of the problem

Explaining the internal structure formation of virialized DM halos, which are studied both observationally and using analytic and numerical simulations, is one of the key cosmological issues.

Despite cosmologists' significant efforts, many aspects of halo formation remain unclear. In particular, it is unclear whether the universal density profile [3]-[5] (hereafter, the Navarro-Frenk-White (NFW) profile), discovered in a wide range of masses and sizes of DM halo formation models, is truly universal. The NFW profile has been found to correspond well to the observed density profiles in galaxy clusters [6], but at the same time it deviates from the observed galactic profiles in many respects (see [7, 8]). This means that many physical factors controlling galaxy formation are not fully taken into account in numerical models.

Numerical calculations of the N-body problem, which have been widely used for many years, are presently a powerful tool to study the formation of the nonlinear structure of the Universe. But numerical models have many restrictions, which stimulates the development of analytic and approximate methods that can reveal and qualitatively characterize the effect of the main physical processes responsible for halo formation. One of the key processes that are difficult to model numerically is the relaxation of matter contracted in a protohalo. To analyze this process, the cosmological small-scale matter velocity and density fields should be taken into account.

In the framework of the widely used spherically symmetric model of the collapse, direct relations between the properties of the initial density perturbations and virialized halos are given by the Press-Schechter relations or their extensions (see [9]-[20]). In this approach, the collapse is described as a consecutive fall of spherical shells, with their subsequent relaxation and redistribution inside the halo. Each spherical layer is characterized by the mass and turn-around radius (the moment of 'decoupling' from the Hubble expansion), which can be related to the spectrum of initial density perturbations, for example, using the smoothing of the density perturbation field by filters of different scales (see [17]). This approach can be generalized to include the

angular momentum of the shells, external tidal forces, an external density distribution, etc. [21]-[26]. Another description of halo formation, which is not based on the quasispherical collapse but uses the Zeldovich approximation, is proposed in [27].

It is well known that the formation of any dense object means the relaxation of contracted matter. In the spherical collapse model, this is the so-called violent relaxation process, which provides the energy and mass redistribution of the compressed matter, the removal of the excess energy from the system, and the halo contraction. The simplest example of the violent relaxation is given by the collapse of a homogeneous nonrotating DM cloud of a finite size (see [28]-[30]). The angular momentum does not stop the violent relaxation [21]-[23], but does weaken it (see, for example, [26, 31]).

In contrast to such methodically transparent results, numerical calculations show that to describe the halo formation process, it is insufficient to consider the fall of only diffusive matter (spherically symmetric or anisotropic). In numerical models, the formation of a halo is accompanied by the formation of random systems of low-mass high-density subhalos and their subsequent coalescence in the main protohalo. This process of hierarchical merger provides the mass transfer inside the main halo, in which small subhalos are ‘stripped’ by the tidal interaction and dynamical friction with the surrounding matter (see [32]-[35]). Both processes – the fall of diffusive matter and the merger of satellite subhalos – play similar roles in the halo formation.

The results of numerical calculations suggest that the merger of early formed high-density subhalos can stimulate the formation and later increase in the central density in the main halo, and the violent relaxation here has a smaller effect. For example, even one merger of subhalos with comparable masses can strongly change the internal structure of the whole halo [36]. The merged subhalos supply the common halo with their kinetic energies and angular momenta, and hence the destruction and stripping of subhalos inside the main halo become the principal constituents of the relaxation process. The interaction of subhalos with the main halo, other subhalos, and diffusive matter redistributes the energy in the main halo and changes its internal structure. The efficiency of relaxation in numerical calculations is comparable with estimates obtained in the simplest spherically symmetric collapse models (see [31, 37, 38]).

The relaxation is needed to provide the energy removal from the main halo, but at the same time it leads to the chaotization of the collected material and largely determines the density profile unification in the relaxed

halos. Nevertheless, in both the hierarchical and spherical halo formation models, the merger of subhalos (or spherical shells) is not purely chaotic and is controlled by the initial density and velocity distributions. During the relaxation, the initial conditions do not smear out completely and are partially conserved. As we show below, both halo mass distribution and their internal structure depend on the initial perturbation spectrum.

It is well known that initial conditions can dramatically affect the evolution of dynamical systems. The difference between the cold and hot dark matter cosmological scenarios provides an example. In the context of halo formation, the possible influence of thermal velocities and small-scale initial perturbations were discussed in [26, 27, 39, 40]. Here, we significantly improve the description of this effect by using statistical characteristics of spatial density and velocity distributions inside a collapsed DM cloud [41]. This approach allows estimating the background entropy of the relaxed matter, which is related to the initial small-scale velocity perturbations, and its dependence on the mass of halos formed. The effect of factors such as the angular momentum of collapsing matter and nonlinear destruction of low-mass subhalos is not considered here. Due to the random character, these factors can only increase the background entropy and its deviation from the mean value. Our calculations yield the minimum level of the background entropy, which, nevertheless, can change the internal structure of the emerging halos and significantly suppress the central DM cusp formation inside them.

The use of the entropy approach in describing relaxed halos allows the determination of the total entropy (initial entropy and that acquired during nonlinear relaxation) of DM particles in the halo. In contrast to the kinetic approach, our method does not appeal to the halo particle distribution and does not describe the relaxation history. But it correctly reproduces any distribution of matter inside a relaxed spherical halo and distinguishes between the properties of this distribution that are due to the initial conditions and those that are related to the relaxation process itself. Such a calculation is possible due to the property of entropy as the most stable characteristic of matter, changing only during irreversible processes.

For both spherical and hierarchical halo formation models, it is possible to estimate the entropy growth during matter relaxation [42]. For the spherical collapse, this estimate can be done analytically (see [28]). The hierarchical relaxation process is more complicated and is not described analytically, and we therefore use the results of numerical calculations to estimate the entropy growth there.

In the observed gravitationally bound objects, the spatial distributions of DM, baryons, and luminous matter are different. In the DM-dominated Universe, it is reasonable to regard the DM halo formation problem as the first approximation to a more complicated problem of the formation of gravitationally bound systems. Here, we consider only the DM dynamics in the CSM framework, ignoring the effect of dark baryons and luminous matter. Nevertheless, in some cases where the effect of the baryon component on the internal structure of a galaxy can be significant (see, e.g., [43]), this issue requires further studies.

### 3 Dark matter halo

We assume DM to consist of nonrelativistic massive particles that interact with each other and other particles only gravitationally. This matter is called ‘dark’ because it is invisible – it has a nonbaryonic nature and does not interact with light.<sup>1</sup> However, DM can be studied using dynamical methods, because it is clumped and produces spatial gradients of the gravitational potential that influence the motion of visible bodies (galaxies, stars, gas), the state of baryons (hot gas), and light ray deflection (gravitational lensing).

The mean DM density in the Universe is five times higher than the density of cosmological baryons, which is why nonrelativistic dark particles control the process of gravitational clustering and of the evolution of the inhomogeneous part of the gravitational potential of the Universe. The density contrast of a weakly inhomogeneous initial spatial DM distribution increases with time. Because this matter is cold, the pressure gradients there are small and cannot prevent the development of gravitational instability.

In regions with enhanced density, the Friedman expansion rate slows down, and at some instant the DM expansion stops and turns into collapse. During dynamical contraction and subsequent oscillations of matter flows, processes of violent collisionless gravitational relaxation occur: particles move in a variable gravitational potential localized in space, such that some particles ( $\sim 10\%$ ) are expelled from the system and carry away the excess positive energy. The remaining energy of the clump is redistributed inside the system, and a gravitationally bound DM object called a halo is formed.

---

<sup>1</sup>Matter can be weakly visible if its particles weakly interact with light, for example, if they annihilate to emit photons in the regions with high DM density in galactic centers.

The observed halos (galaxies, their groups, and clusters) are relaxed systems of particles that are gravitationally bound in all three spatial directions. The upper limits of the halo sizes and masses are a few Mpc and  $10^{15}M_{\odot}$ . We recall that the mass of matter in the Universe in a sphere with a radius  $R = 10$  Mpc is  $M_{10} \simeq 1.6 \cdot 10^{14}M_{\odot}$  [see Section 8, formula (21)]. Here and below in numerical estimates, we assume the CSM parameters

$$\begin{aligned} \Omega_{\text{m}} \equiv \frac{\rho_{\text{m}}}{\rho_{\text{c}}} &= 1 - \Omega_{\text{E}} \simeq 0.3, & \rho_{\text{c}} &= \frac{3H_0^2}{8\pi G} \simeq 10^{-29} \text{ g cm}^{-3}, \\ H_0 &\simeq 70 \text{ km s}^{-1} \text{ Mpc}^{-1}, \end{aligned} \quad (1)$$

where  $\rho_{\text{m}}$  is the cosmological DM density,  $\rho_{\text{c}}$  is the critical density in the Universe,  $\Omega_{\text{E}}$  is the cosmological density of dark energy expressed in units of the critical density,  $H_0$  is the Hubble constant, and  $G$  is the gravitational constant.

We consider the simplest equilibrium conditions of self-gravitating DM systems. The distribution function of non-relativistic particles in a spherically symmetric halo depends on the radial distance to the halo center  $r$  and moduli of the radial and transverse particle momenta. In spherical coordinates, the stress-energy tensor of matter takes the diagonal form

$$T_{\mu}^{\nu} = \rho \text{diag} (1, -\sigma_r^2, -\sigma_t^2, -\sigma_t^2), \quad (2)$$

where  $\rho = \rho(r)$  is the halo density profile, and  $\sigma_r(r)$  and  $\sigma_t(r)$  are the radial and transverse velocity dispersions of particles. In the Newtonian limit, the identity  $T_{\mu;\nu}^{\nu} = 0$  implies the hydrostatic equilibrium equation for collisionless particles:

$$-\frac{1}{\rho r^2} \frac{d}{dr} (\rho r^2 \sigma_r^2) + \frac{2}{r} \sigma_t^2 = \frac{d\Phi}{dr} = \frac{GM(r)}{r^2}, \quad (3)$$

where the gravitational potential  $\Phi$ , defined up to an additive constant, and the mass of the system  $M$ , which depends on  $r$ , are related to density as

$$\Delta\Phi \equiv \frac{1}{r^2} \frac{d}{dr} \left( r^2 \frac{d\Phi}{dr} \right) = 4\pi G\rho, \quad M(r) = 4\pi \int_0^r \rho r^2 dr. \quad (4)$$

Inside the halo, DM particles move along different orbits, from radial to circular ones. Each orbit is characterized by the energy and angular momentum vector, which are integrals of motion in a static spherically symmetric

field. The density distribution at the halo center can be conveniently characterized by a power-law function,

$$\rho \propto r^{-\alpha} \tag{5}$$

with the exponent (slope)  $\alpha = \text{const} \in (0; 2.5)$ . The particle distribution function depends on the evolutionary history of the halo. Numerical experiments and observations show that for most of the spherical halos, the particle velocity distribution is nearly isotropic, although deviations from isotropy can sometimes be as high as 20–30% (see, for example, [44]).

Large-mass halos do not have enough time to form in the Universe. For example, systems collapsed in one or two dimensions, which are called walls and filaments, are typical nonlinear elements of the large-scale structure of the Universe. On average in the Universe, the density contrast on scales exceeding dozen Megaparsecs remains smaller than unity ( $|\delta\rho/\rho| < 1$ ), and we can consider only regions with an increased or decreased (in comparison with the mean cosmological) density of matter.

## 4 Entropy of particles in the halo

We consider an isotropic distribution of DM particles with  $\sigma_r = \sigma_t = \sigma$  in more detail. The halo equilibrium is determined by the balance of the effective pressure gradient of nonrelativistic matter,

$$p = nT = \rho\sigma^2 \tag{6}$$

and the gravitation produced by the total mass  $M = M(r)$  [see (3)],

$$\frac{dp}{\rho dr} = -\frac{GM(r)}{r^2}, \tag{7}$$

where radial functions  $n = \rho/m$  and  $T$  are the density and effective temperature of particles with the mass  $m = \text{const}$ . By virtue of the equivalence principle,  $m$  cannot be determined from gravitational equations because particles are moving along geodesics irrespective of their masses. The measurable variables are the density  $\rho$  and the particle velocity dispersion  $\sigma$ .

From the hydrostatic equilibrium equation, it is possible to find the radial matter density profile in the halo using the known velocity dispersion distribution  $\sigma(r)$ ; vice versa, using the density distribution, we can reconstruct

the velocity dispersion law. For the adiabatic density distribution,  $\sigma \propto n^{1/3}$ , where the coefficient of proportionality depends on the entropy distribution. In analogy with an ideal gas, we introduce the entropy function  $E = E(r)$  of the virialized halo as [2, 41]

$$E = \sigma^2 \left( \frac{m_p}{\rho} \right)^{2/3} \propto \frac{T}{n^{2/3}} = \frac{p}{n^{5/3}}, \quad (8)$$

where  $m_p$  is the mass of a proton to which the halo particle mass  $m$  is normalized.

The function  $E(r)$  is the measure of the total entropy of halo particles acquired during the full halo formation history.<sup>2</sup> It mainly includes the background entropy determined by the initial small-scale flows and matter inhomogeneities in the protohalo, and the acquired entropy generated during collisionless and hierarchical relaxation of matter at the nonlinear stage of the halo formation.

## 5 Isothermal sphere

Modeling the internal structure of observed halos frequently involves the isothermal sphere approximation, where the velocity dispersion can be assumed constant and independent of the radius:

$$\sigma(r) = \sigma_0 = \text{const}, \quad \kappa_0 \equiv \frac{4\pi G}{\sigma_0^2} = \frac{4\pi G m}{T} = \text{const}. \quad (9)$$

This approximation is in good agreement with observational data in a restricted range of scales (Fig. 1).

After multiplying Eqn (7) by  $r^2$  and differentiating with respect to  $r$ , we obtain the equation for the density profile in an isothermal sphere:

$$\frac{d}{\rho r^2 dr} \left( \frac{r^2 d\rho}{\rho dr} \right) = -\kappa_0. \quad (10)$$

---

<sup>2</sup>We stress that  $E$  is a function of entropy and not the entropy itself. Here, we do not consider general issues of the applicability of the notion of entropy (coarse-grained entropy, see footnote 3) to collisionless particles, by defining the function  $E(r)$  only for stationary equilibrium systems with isotropic particle velocity distributions. We recall that in definition (8),  $\sigma^2 = \overline{v^2}$ , where  $v$  is the one-dimensional peculiar velocity of dark matter particles at a point  $r$  (the bar means averaging over the velocity space).

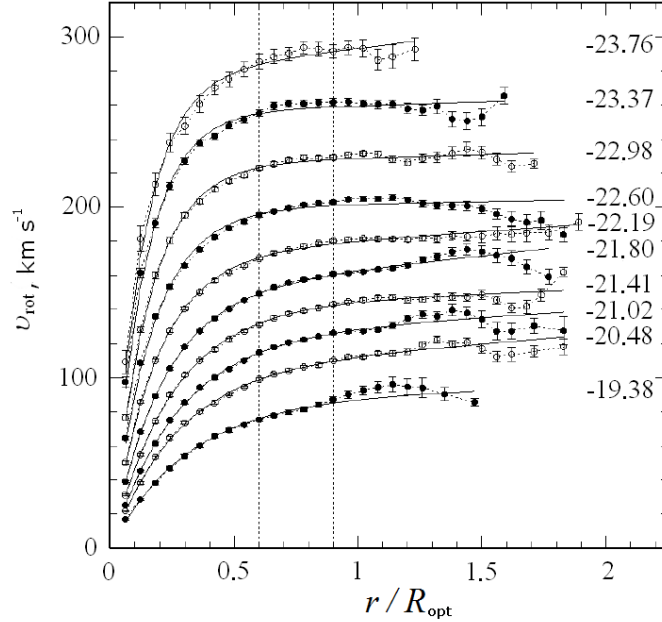


Figure 1: Rotation curves for 2155 galaxies (from [45]). The curves, which are divided into several groups in accordance with the galaxy luminosities, are characterized by the absolute stellar magnitude in the I-filter (shown to the right).  $R_{\text{opt}}$  is the ‘optical’ radius of galaxies, inside which 83% of the integral emission flux is contained.

This nonlinear equation contains an attractor – a particular solution that is an attracting separatrix for dynamical trajectories (10). The general solution has the form

$$\rho(r) = \begin{cases} \frac{\rho_0}{1 + r^2/(2r_0^2)}, & r < r_0 \equiv \sqrt{\frac{3}{\kappa_0\rho_0}} \\ \frac{2}{\kappa_0 r^2}, & r > r_0 \quad (\text{attractor}), \end{cases} \quad (11)$$

where the parameter  $\rho_0$  determines the central density of the halo core and  $r_0$  is the characteristic size of the core. Irrespective of the value of  $\rho_0$ , the density profile and mass of the halo at  $r > r_0$  are determined only by the

velocity dispersion of particles:

$$M = \frac{8\pi r}{\kappa_0} \simeq 7 \cdot 10^{12} \left( \frac{\sigma}{300 \text{ km c}^{-1}} \right)^2 \left( \frac{r}{200 \text{ kpc}} \right) M_\odot. \quad (12)$$

For the characteristic values of  $\sigma$  and  $r$ , we obtain the typical mass of non-linear dark matter halos in the observed Universe – that of galaxy groups. We recall that the total mass of the Local Group, which includes the Milky Way and the Andromeda Nebula, is  $2 \cdot 10^{12} M_\odot$ .

We have derived Eqns (3) and (7) for DM by assuming its dominance; however, these equations can be used to describe hydrostatic equilibrium of any matter (DM, stars, gas) in the gravitational field of the total mass  $M(r)$ . For this, the corresponding  $p$  and  $\rho$  should be substituted in the left-hand side of Eqns (3) and (7). For example, we can rewrite the halo mass in terms of the effective gas temperature  $T_{\text{gas}}$  in the equilibrium:

$$M = \frac{2T_{\text{gas}} r}{G\mu_{\text{gas}}} \simeq 7 \cdot 10^{12} \left( \frac{T_{\text{gas}}}{1 \text{ keV}} \right) \left( \frac{r}{200 \text{ kpc}} \right) M_\odot, \quad (13)$$

where  $\mu_{\text{gas}} \simeq m_p = 1 \text{ GeV}$  is the molecular weight of the gas. Such a hot gas, which has been present in galaxy clusters for several billion years, is observed by X-ray telescopes, which allows reconstructing the gravitational potential distribution and estimating the total mass of clusters (see, e.g., [46]).

We return to solution (11). The core density  $\rho \simeq \rho_0$  does not relate to the gravity of matter: it depends only on the initial cosmological conditions that determined the halo formation history. The size of the core is determined by the product of the particle velocity and the dynamical time of the central density:

$$r_0 \simeq \frac{\sigma_0}{2\sqrt{G\rho_0}}.$$

Here,  $r_0$  is the radius at which the matter self-gravity becomes significant. At  $r > r_0$ , the dark matter gravity restructures the inner halo such that the rotation velocities of particles cease to depend on the radius:

$$v_{\text{rot}}(> r_0) = \sqrt{\frac{GM}{r}} = \sqrt{2}\sigma_0 = \text{const}. \quad (14)$$

Such velocity distributions are realized in many gravitationally bound cosmological objects. For example, flat rotation curves are observed in spiral galaxies (Fig. 2): circular velocities of stars and gas first increase as the

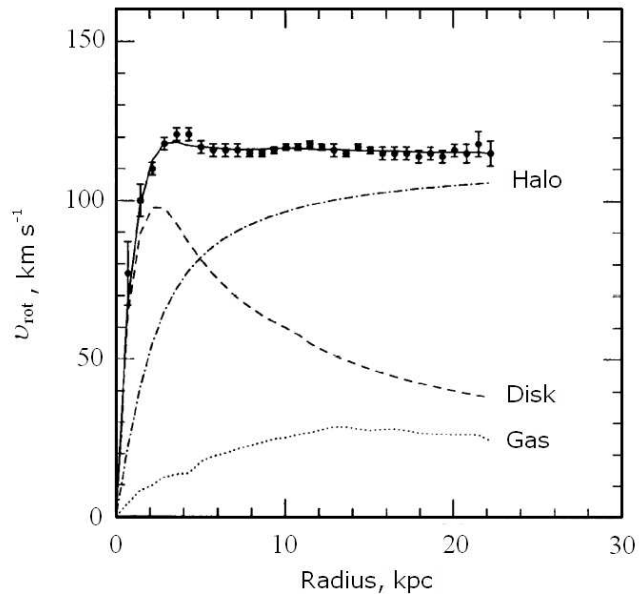


Figure 2: The rotation curve of galaxy NGC 6503 (data from [47]). The dark matter halo contribution is shown by the dashed-dotted line.

radius increases and then become constant or change very slowly. The DM mass increasingly contributes at large distances and maintains the flat part of the rotation curve over about ten dynamical scales.

Dwarf galaxies with low surface brightness (Fig. 3) provide another example. There, DM dominates starting from small radii, and a linear increase in the circular rotation velocity is observed, suggesting a small variation of the DM density in the central core [see (18)]. We see that the initial increase of rotation curves also corresponds to isothermal sphere (11):

$$v_{\text{rot}}(< r_0) = \sqrt{\frac{GM}{r}} = \frac{\sigma_0 r}{r_0}. \quad (15)$$

The fact that the inner circular velocities are smaller than the particle velocities in the halo ( $v_{\text{rot}} < \sigma_0$ ) suggests that the halo particles freely, by inertia, move over the region  $r \sim r_0$  with a constant velocity and do not feel gravity.

To within the observational accuracy, isothermal sphere distribution (11)

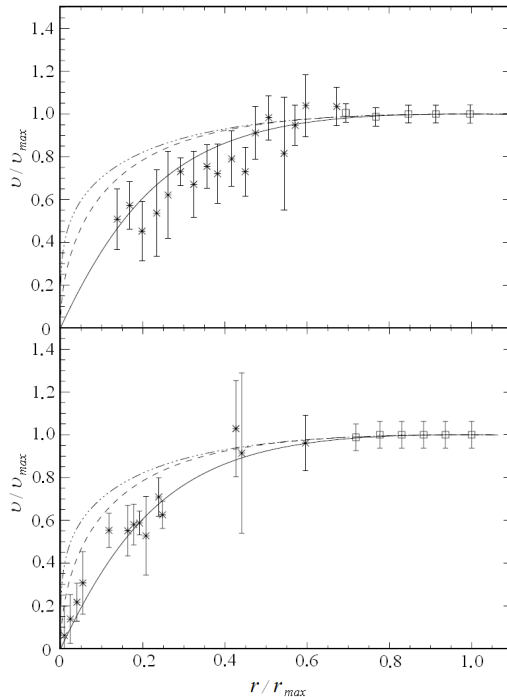


Figure 3: The circular rotation velocity as a function of radius in low-brightness surface galaxies (a) LSB F571-8 and (b) LSB F583-1. The solid curve shows the Burkert approximation, the dashed curve shows the NFW approximation, and the dashed-dotted line shows the Moore profile (data from [48]).

can be approximated by the simple formula

$$\rho \simeq \frac{\rho_0}{1+x^2}, \quad x = \frac{r}{r_0}. \quad (16)$$

The flat part of the circular velocity, corresponding to the linear mass increase  $M \propto r$  [see (14)], is observed within a finite dynamic range. The density distribution in such a system can be conveniently described by the profile

$$\rho \propto \frac{1}{(1+x^2)(r+r_s)}, \quad (17)$$

where  $r_s = \text{const}$  is a characteristic cut-off parameter. In the central part at  $r < r_s$ , the profile is close to that of the isothermal sphere in (16); but

at large distances, the density decreases  $\propto r^{-3}$  and circular velocities slowly decrease. The circular velocity reaches a maximum in the region with the local density slope exponent is  $\alpha \simeq 2$ .

## 6 Internal halo structure

The radial dependence of the circular velocity is related to the density distribution inside the halo. Figure 3 demonstrates rotation curves of dwarf galaxies that can be approximated well by phenomenological profile (17) with  $r_s = r_0$ , which is referred to as the Burkert approximation [49]:

$$\rho \propto \frac{1}{(1+x^2)(r+r_0)}. \quad (18)$$

Similar examples of galactic cores with slowly changing density are typical for small galaxies. So far they have not been reproduced in numerical calculations of structure formation.

The nonlinear relaxation of a contracting cloud leads to a diverging central density in the forming halo. Analytic models of the collapse [28, 29] consider the gravitational contraction of a spherical cloud at rest with a smooth density distribution. After the relaxation, a singular halo density profile is formed with the slope exponent  $\alpha \sim 1.6 - 2$ . This result, which is also confirmed by numerical calculations [50]-[52], is closely related to the choice of the initial state of the contracting mass, namely, to the absence of random small-scale velocities and an almost spherically symmetric density distribution. This example very well illustrates the transformation of the kinetic energy of the contracting cloud into thermal energy of the halo during violent relaxation.

More realistic models of the collapse with subsequent DM relaxation appear in numerical modeling of the evolution of a system of gravitationally interacting  $N$  bodies ( $N \sim 10^{10}$ ). Here, random initial particle velocities, the anisotropy of the contraction, and the successive merger of the main halo and its satellites are taken into account. The mean density profile of halos formed in these calculations is described by the NFW approximation [3]-[5], which depends on a single parameter  $r_s$  and has the form

$$\rho \propto \frac{1}{r(r+r_s)^2}. \quad (19)$$

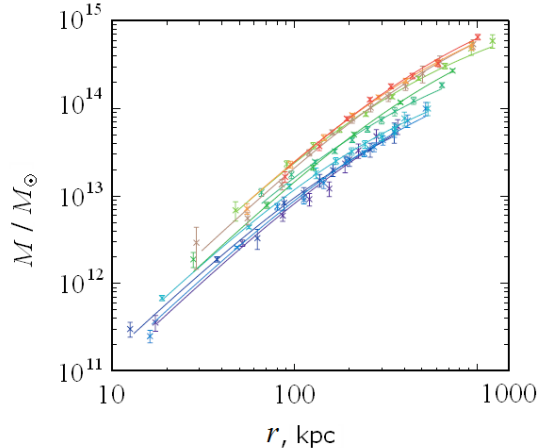


Figure 4: Dark matter mass distribution in galaxy clusters according to the data in [6].

At  $r < r_s$ , the dependence of the mean density profile on  $r$  tends asymptotically to a cusp-like power law with the slope  $\alpha = 1$ .

The NFW profile obtained in numerical  $N$ -body models well describes the density distribution in galaxy clusters (Fig. 4, 5). It should be remembered, however, that this profile is obtained by averaging density distributions of many halos, and deviations of individual profiles from the mean one can exceed 20% (Fig. 6). We also note that technical limitations restrict the dynamical range of model scales, and the properties of halos with low and moderate masses are not properly reproduced in the calculations. Numerical constraints also restrict the size of the central region resolved in numerical models.

In numerical models, the DM halo central density tends to infinity, but the mass remains finite and tidal forces are insignificant. Such an internal structure was called the halo central cusp. Thus, singular cusps are formed in numerical models, but these structures are not observed in the Universe.

Figure 7 demonstrates the rapid density increase in a DM halo that appears in numerical models. The comparison with observed galactic profiles is shown in Fig. 8. The question of whether DM cusps exist in reality is important not only for understanding galaxy formation; it also can be connected with the physics of DM particles. For example, one of the methods to search

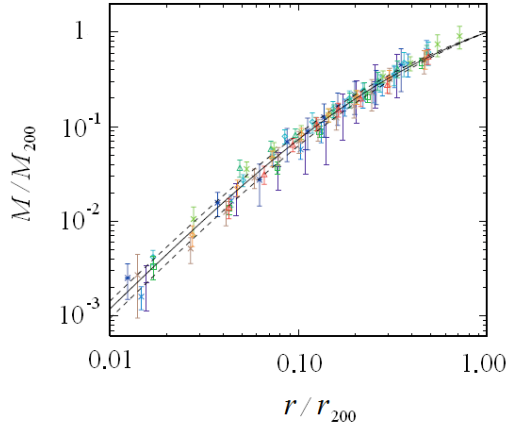


Figure 5: The curves shown in Fig. 4 in variables normalized to the mass and radius of the sphere inside which the mean density is 200 times as high as the matter density in the Universe. The solid line shows the NFW approximation.

for possible DM particle annihilation assumes that central cusps do exist in galactic centers.

To summarize, the comparison of the observed galaxies with numerical models leads to the following conclusions.

(1) Numerical models reproduce the formation of massive objects, and the density profile of galaxy clusters is in good agreement with calculations.

(2) Burkert profile (18) is mainly observed in low- and moderate-mass galaxies dominated by DM. The formation of such galaxies is related to the initial perturbations of comparatively moderate scales. In the central regions of more massive spiral galaxies, the DM and baryon densities are comparable and it is difficult to separate them.

(3) These issues are closely related to the number count of our Galaxy satellites. Until recently, the number of the observed satellites was about two times less than predicted by numerical models [44]. However, many very faint satellites have been discovered recently, and their number even exceeds the prediction of numerical models (see [56]-[60]). This shows that the properties of low-mass objects need to be studied further.

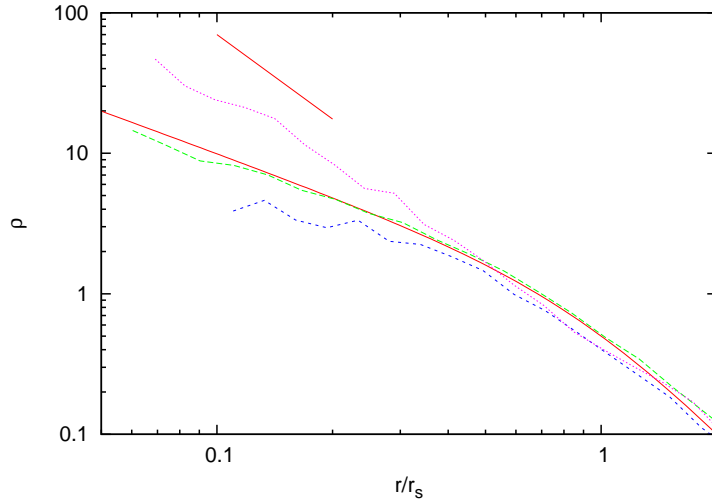


Figure 6: The density profiles of three halos with masses  $10^{12} - 10^{13}$  obtained in numerical models [53]. The solid curve in the center shows the NFW profile. The short line in the upper part of the figure corresponds to the slope  $\alpha = 2$ .

## 7 What is needed to form cusps

Do singular cusps that appear in numerical experiments actually form in Nature? To answer this question, it is necessary to understand the structure of cusps and what their formation conditions should be.

As we discerned from the isothermal sphere example, DM particles freely intersect the core region  $r < r_0$  and do not stay there. This conclusion is valid for much more numerous halos with a small central mass ( $\alpha < 1$ ), because the gravitational force tends to zero at small radii:

$$\frac{GM(r)}{r^2} \propto r^{1-\alpha} \rightarrow 0 \quad \text{as} \quad r \rightarrow 0. \quad (20)$$

Conversely, more massive cusps ( $\alpha > 1$ ) gravitationally influence DM particles and keep them inside the halo. Clearly, velocities of the kept particles must be sufficiently low for the particles to remain in the cusp region. Therefore, to form a cusp, it is necessary to collect many cold particles in its center. At least two questions arise.

- Where can cold particles in the perturbation field be found?

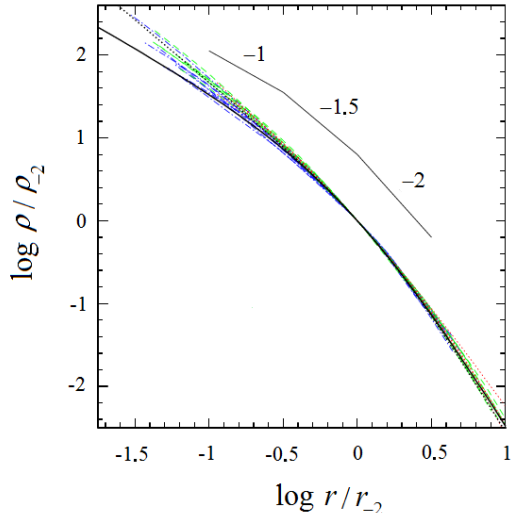


Figure 7: (See color version at [www.ufn.ru](http://www.ufn.ru)). The mean halo density profiles in numerical models [54]. Dwarf galaxies are shown in red, intermediate mass galaxies are shown in green, and galaxy clusters are shown in blue. Numbers show the power-law slope exponents  $d \ln \rho / d \ln r$ ; the normalization corresponds to the slope point  $-2$ .

- How can cold particles be transported to the central part of the halo without being heated?

Because the fraction of energy removed during halo formation does not exceed 10-15% and the degree of matter contraction during relaxation is finite, both these questions should be first of all addressed by numerical programs for N-body calculations: where is the ‘cooler’ of DM particles and why is their ‘warming up’ by small-scale cosmological motions of matter not taken into account in calculations?

We know that in the absence of small-scale perturbations, cusps are formed in models of quasispherical collapse (see Section 6). In these analytic calculations, all particles are initially focused toward the center (by the chosen initial conditions), and a significant fraction of the particles, by crossing the center, cools due to violent relaxation and remains inside the cusp. But in real cosmological conditions, DM particles are ‘defocused’ by small-scale perturbations and hence do not pass through the center. In ad-

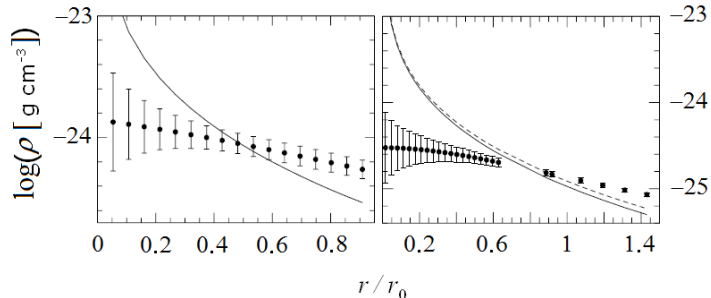


Figure 8: Demonstration of the cusp problem in galactic DM halos (data from [55]). The symbols show the observed galactic density profiles in (a) DDO 47 and (b) ESO 287-G13, the curves show the mean density profiles obtained in numerical modeling.

dition, the fall of DM clumps and their merging ‘stir up’ the central region and hamper effective particle cooling.

Of course, the quantitative characteristics of these mutually opposite processes must be calculated and checked numerically; however, modern numerical modeling is not perfect and needs to be improved.

First of all, it is required to control DM motions in a wide range of scales, from large cosmological scales on which the initial particle distributions are given, to very small ones, which allows the inner regions of the forming halos to be resolved. In modern numerical models, the mass resolution, as a rule, does not exceed  $10^7 M_{\odot}$ , which is insufficient to describe the structure of DM cores. Due to the restricted resolution in numerical models, the initial particle distributions have no small-scale perturbations, i.e., there is an effective cut-off of the perturbation spectrum at short wavelengths. The consecutive resolution of selected volumes by the addition of ‘new points’ inside them at the late stage of the evolution (the so-called adaptive method) does not help either, because this procedure does not add necessary information on the initial small-scale field of cosmological perturbations.

A more sophisticated method is sometimes used that involves consecutive recalculation of the model upon adding new particles in the future dense halo regions. This procedure enables small-scale perturbations to be included in the calculation in restricted volumes. But such a recalculation complicates the problem and strongly increases the computation time. The problem of

cusps has not yet been solved. Perhaps this example shows a limitation of the CSM, in which DM particles are considered to be cold. In the CSM framework, we cannot resolve the contradiction between observational data and the results of numerical calculations. The point is that cusps emerge during relaxation of the initially cold matter, in which large-scale particle flows self-intersect to form caustics, from which a cusp is later formed. But the real DM can be initially warm with small random particle velocities. In that case, caustics smear out, and cores with a smoother density distribution are formed in halo centers instead of cusps.

Warm DM can be regarded as an additional parameter of the cosmological model. The mass of warm DM particles that is required to solve the problem of cusps must be not large ( $\sim 10$  keV), which allows the particles to preserve the residual thermal velocities associated with the hot phase of evolution in the early universe. Another possibility of the initial ‘heating up’ of DM particles can be related to the presence of excess power in the perturbation spectrum at small wavelengths. We recall in this connection that the spectrum is fairly well determined on scales above several Mpc from observations of the cosmic microwave background and large-scale galaxy distribution. At the same time, at small scales, the spectrum of initial perturbations can deviate from a power law, which can in turn affect the structure of small galaxies.

These assumptions, however, go beyond the CSM framework. Our approach is different. We believe that there are currently no strong grounds to complicate the fundamental model, and the problem can have a simpler solution, which does not require modification of the CSM. The influence of small-scale velocity and density perturbations on the internal halo structure can be studied analytically using entropy function (8). The use of entropy instead of density is motivated by the fact that for most particles, the entropy increases during the halo formation and relaxation and is an integral characteristic of the entire halo formation history. Evaporation of particles during relaxation decreases the entropy, but this effect is rather small.

By definition, DM particles are initially cold, i.e., their entropy is zero. On the other hand, there are random small-scale flows and matter clumps, which are tidally destructed and scattered when approaching each other inside collapsing protohalos to form folds and intersections, thus heating DM particles and chaoticizing their velocities before the violent relaxation begins. Therefore, during the first contraction, the small-scale velocity perturbations in the protohalo are transformed into chaotic motions of DM particles. This

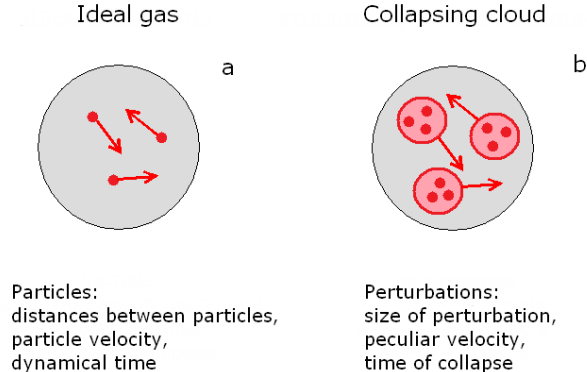


Figure 9: Motion of particles in (a) an ideal gas and (b) a DM protohalo [2]. The entropy of particles in the region of size  $r$  is determined on the dynamical time scale coincident with the collapse time:  $r/v \simeq H^{-1}$ .

process can be described in terms of coarse-grained entropy, in analogy with the description of the ideal gas [41].

## 8 Ensemble of protohalos

To introduce the entropy characteristic of particles in a protohalo, the notion of an ensemble is needed. It can be introduced as a subsample of the field of linear perturbations embracing all spatially bound regions that collapse by the time corresponding to the current redshift  $z$ . A schematic comparison with an ideal gas is shown in Fig. 9.

A protohalo is characterized by the mass  $M_R$  first collapsing at the redshift  $z$ , which is called the instant of halo formation. The mass  $M_R$  corresponds to the linear comoving size  $R$ :

$$M_R = \frac{4\pi}{3} \rho_m R^3. \quad (21)$$

A sphere with the radius  $R = 10$  Mpc comprises the typical galaxy cluster mass  $M_{10} \simeq 1.6 \cdot 10^{14} M_\odot$  (see Section 3).

To single out a protohalo from the common density field, it is necessary that the protohalo have an initial threshold mass excess in the sphere of

radius  $R$  which provides the total negative binding energy of this region and ensures its collapse by the given time instant (see Appendix A):

$$\nu_R \equiv \frac{\delta_R}{\sigma_R} \geq \nu \equiv \frac{\delta_c(z)}{\sigma_R}. \quad (22)$$

The function  $\delta_c(z)$ , which can be calculated analytically, is controlled numerically. In the CSM,  $\delta_c = \bar{g}(z) \cdot \delta_c(z) = \text{const} \simeq 1.67$ , where  $\bar{g}(z)$  is the growth factor of linear density perturbations ( $\bar{g}(0) = 1$ ). The initial ensemble of protohalos of interest here, with initial masses

$$M_h \geq M_R \quad (23)$$

includes only those space points  $\mathbf{x}$  for which the mean matter density inside a sphere of the radius  $R$  around the given point increases the threshold value in (22), where  $\delta(\mathbf{x}) \equiv \rho(\mathbf{x})/\rho_m - 1$  is the linear density contrast relative to the mean density in the Universe  $\rho_m$ ; the smoothed density contrast  $\delta_R$  with the filter of radius  $R$  is

$$\delta_R = \delta_R(\mathbf{x}) = \int \delta(\mathbf{x}') W_R(|\mathbf{x} - \mathbf{x}'|) d\mathbf{x}', \quad (24)$$

where  $W_R(r)$  is the ‘window’ function

$$W_R(r) = \frac{3}{4\pi R^3} \begin{cases} 1, & r \leq R \\ 0, & r > R \end{cases}$$

Clearly, function (24) contains no information on perturbations on scales smaller than  $R$ . The variance of the smoothed density linear contrast  $\sigma_R$ , linearly approximated to the present moment  $z = 0$ , is related to the power spectrum of inhomogeneities  $P(k)$  by the integral relation (see Appendix A)

$$\sigma_R^2 \equiv \langle \delta_R^2 \rangle = \int_0^\infty P(k) W^2(kR) k^2 dk, \quad (25)$$

where  $W(y) = 3y^{-3}(\sin y - y \cos y)$  is the Fourier transform of the window function ( $y = kR$ ). It is known from observations that  $\sigma_{11} \simeq 0.8$  for the radius  $R = 11$  Mpc, comprising the galaxy cluster mass  $M_{11} \simeq 2 \cdot 10^{14} M_\odot$ . In astronomy, it is equivalent to the historically established normalization to ‘sigma eight’, where the index ‘eight’ corresponds to the physical radius  $R = 8/0.7$  Mpc  $\simeq 11$  Mpc.

We use the obtained ensembles to describe the mean ‘thermodynamic’ characteristics of DM in protohalos. The total entropy of a virialized halo integrates the joint effect of all nonequilibrium processes that occurred during the entire halo formation time, including both the background particle (coarse-grained) entropy related to the initial cosmological perturbations and the acquired entropy generated during the violent relaxation and hierarchical clustering of matter. The cosmological part can be calculated analytically, and to estimate the nonlinear component, we use numerical results.

## 9 From density profile to entropy

First of all, it should be understood how the entropy is distributed inside an equilibrium halo. To simplify calculations, we restrict ourselves by considering the power-law approximation of the central halo density profile (5):

$$\rho(r) \propto r^{-\alpha}, \quad (26)$$

$$M(r) = 4\pi \int_0^r \rho(x) x^2 dx \propto r^{3-\alpha},$$

with the slope exponent  $\alpha \in (0; 2.5)$ . In numerical calculations of the halo formation, profiles with  $\alpha \gtrsim 1$  emerge, while observations typically show that  $\alpha < 1$  (Fig. 10). In the first case, we are dealing with a cusp ( $1 \leq \alpha < 2.5$ ) and in the second case, with a core ( $0 \leq \alpha < 1$ ).

The physical difference between the cusp and the core follows from the behavior of the effective pressure, which can be determined from Eqn (7):

$$p(r) = c_1 + c_2 r^{2(1-\alpha)}, \quad (27)$$

where  $c_1$  and  $c_2$  are integration constants. The critical slope is  $\alpha = 1$ : in a core, the pressure is finite, while in a cusp it diverges at the center.

From Eqn (8), we obtain the entropy mass function

$$E(M) \propto c_1 M^{\beta_1} + c_2 M^{\beta_2} \propto M^\beta, \quad (28)$$

$$\beta_1 = \frac{5\alpha}{3(3-\alpha)}, \quad \beta_2 = \frac{6-\alpha}{3(3-\alpha)},$$

where the parameter  $\beta = d \ln E / d \ln M$  lies in the range between  $\beta_1$  and  $\beta_2$  and its local value depends on the current mass of the halo. At  $\alpha = \alpha_c \equiv 1$ ,

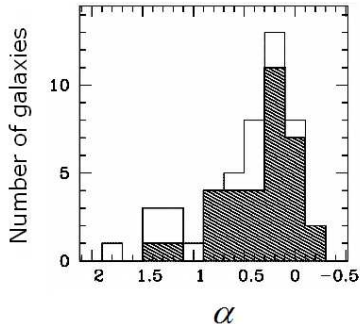


Figure 10: Distribution of the power-law exponent  $\alpha$  in the central part of galaxies with a low surface brightness (see [61]).

the interval of possible values of  $\beta$  contracts to the point

$$\beta_1 = \beta_2 = \beta_c \equiv \frac{5}{6}.$$

We have passed from the radius  $r$  to the comoving mass  $M$  in the sphere of radius  $r$  because this mass is conserved during both linear perturbations and the halo relaxation.

As stressed above, the entropy mass function accumulates the action of irreversible processes during DM evolution and determines the equilibrium halo density profile. In the considered range of  $\alpha$ , we have  $\beta_{1,2} > 0$ , and hence  $E(M) \rightarrow 0$  as  $M \rightarrow 0$  (Fig. 11). But in the cusp center, the entropy of particles is very small,

$$\beta > 5/6 : \quad M^{-5/6} E(M) \rightarrow 0 \quad \text{as} \quad M \rightarrow 0,$$

while in the core center it is much higher, which makes the cusp formation impossible,

$$\beta < 5/6 : \quad M^{-5/6} E(M) \rightarrow \infty \quad \text{as} \quad M \rightarrow 0.$$

For the critical value  $\beta = 5/6$ , it follows from (8) and (28) that

$$M \propto \sigma^4. \tag{29}$$

This formula reproduces the well-known empirical Faber–Jackson [62] and Tully–Fisher [63] relations, which relate the observed velocity dispersion of

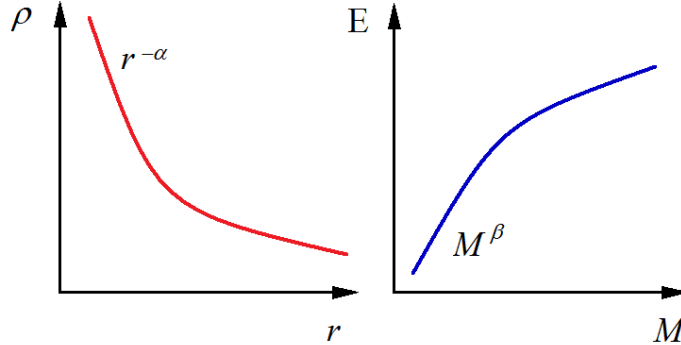


Figure 11: Profiles of (a) the density and (b) the entropy in a DM halo [2].

stars or gas to the mass (luminosity) in elliptical galaxies or spherical sub-systems of spiral galaxies.

Figure 12 illustrates the difference between the cusp and the core of an equilibrium halo from the standpoint of the entropy distribution. It follows that the formation of the central cusp or core depends on the total entropy of matter acquired before the formation of the halo, during and after its formation.

We can now quantitatively answer the question as to how the initially cold DM particles of the CSM acquire a nonzero temperature.

The halo formation process can be divided into several consecutive stages.

- Initial DM motions are potential and are correlated, relative velocities of close particles are small, and the DM velocity field is smooth. Random deviations from the mean velocity determined by the initial perturbations spectrum increase with increasing the scale to saturate at relatively large scales ( $\sim 40$  Mpc) (see Fig. 14 in Section 10).
- During contraction of a protohalo, particles approach each other and mix at small scales, and the initial phase of the small-scale part of the random velocity is lost: DM particles heat up (the background entropy mass function  $E_b$  arises).<sup>3</sup>
- The chaotization of the regular contraction rate and transformation of the kinetic energy of the contraction into thermal energy occur some-

---

<sup>3</sup>Coarse-grained entropy can be defined as the fraction of the phase space volume per

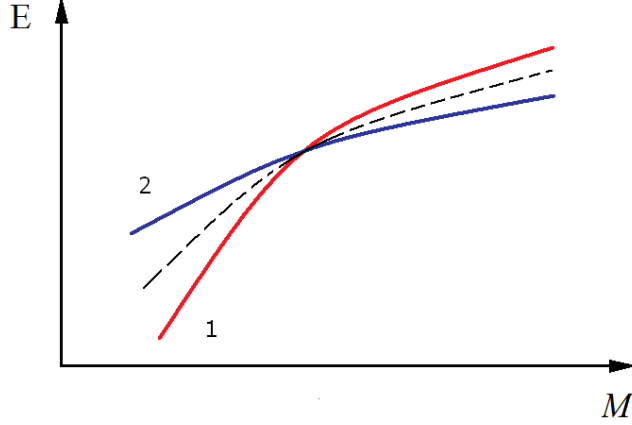


Figure 12: The entropy mass function of an equilibrium halo. Curve 1 shows the cusp, curve 2 shows the core, and the dashed curve corresponds to  $\beta_c = 5/6$ .

what later during violent relaxation and merger of clumps (the entropy  $E_g$  is generated).

- The resulting density profile of equilibrium halos is obtained by adding the initial entropy  $E_b$  and the acquired entropy  $E_g$ .

In Sections 10 and 11, we obtain the initial mean entropy profile  $\langle E_b \rangle$  using the corresponding dispersion of linear velocity perturbations [see Section 11, formula (49)]. This representation assumes an almost adiabatic contraction of matter and gives the lower limit of the mean function  $E_b(M)$  at small  $M$ .

---

particle:

$$E_b \propto \left( \frac{\Delta N}{\Delta \mathbf{x} \Delta \mathbf{v}} \right)^{-2/3} \simeq \frac{\sigma_{\Delta \mathbf{v}}^2}{n^{2/3}},$$

where  $\Delta N$  is the number of particles in the volume  $\Delta \mathbf{x} = \Delta x_1 \Delta x_2 \Delta x_3$ , including the oppositely directed particle flows,  $\Delta v_i$  is the relative particle flow velocity on the scale  $\Delta x_i$  ( $\Delta \mathbf{v} = \Delta v_1 \Delta v_2 \Delta v_3$ ), and  $\sigma_{\Delta \mathbf{v}}$  is the dispersion of relative particle flow velocities inside the volume  $\Delta \mathbf{x}$ . The coarse-grained entropy does not decrease during relaxation of particle flows and is transformed into the real entropy mass function of the virialized system.

## 10 Initial cosmological perturbations

The field of scalar cosmological perturbations is characterized by three gauge-invariant variables: the space vector of the shift of a material point from the unperturbed position

$$\mathbf{S} = \mathbf{S}(\mathbf{x}), \quad (30)$$

the total velocity of matter

$$\mathbf{V} = \mathbf{V}(z, \mathbf{x}), \quad (31)$$

and the comoving density perturbation

$$\delta_m \equiv \frac{\rho(z, \mathbf{x})}{\rho(z)} - 1 = \bar{g}(z) \cdot \delta(\mathbf{x}). \quad (32)$$

The dependence of the mean density on the redshift has the form  $\rho(z) = \rho_m (1+z)^3$ , where the DM density is given by (see Section 3)

$$\rho_m = \frac{3\Omega_m H_0^2}{8\pi G} \simeq 3 \cdot 10^{-30} \frac{\text{g}}{\text{sm}^3}.$$

The mean particle shift in the Universe is zero, and its dispersion is determined by the integral of the power spectrum of density perturbations:

$$\sigma_{\mathbf{S}} \equiv \sqrt{\langle \mathbf{S}^2 \rangle} = \left( \int_0^\infty P(k) dk \right)^{1/2} \simeq 14 \text{ Mpc}. \quad (33)$$

A sphere with the radius  $R = \sigma_{\mathbf{S}}$  contains the mass of a rich galaxy cluster

$$M_{\mathbf{S}} = \frac{4\pi}{3} \rho_m \sigma_{\mathbf{S}}^3 \simeq 4 \cdot 10^{14} M_\odot.$$

Relations between variables are determined by the linear perturbation theory (see [1] for more details):

$$\mathbf{r}(z, \mathbf{x}) = (1+z)^{-1} (\mathbf{x} + \bar{g}\mathbf{S}), \quad (34)$$

$$\mathbf{V} \equiv \dot{\mathbf{r}} = H (\mathbf{r} - \bar{g}'_z \mathbf{S}), \quad \delta(\mathbf{x}) = -\text{div } \mathbf{S}, \quad (35)$$

$$\mathbf{v} \equiv \mathbf{V} - H\mathbf{r} = -H\bar{g}'_z \mathbf{S}, \quad \sigma_{\mathbf{v}} \equiv \sqrt{\langle \mathbf{v}^2 \rangle} \simeq 200 \sqrt{\frac{10}{1+z}} \frac{\text{km}}{\text{s}}, \quad (36)$$

where  $\mathbf{r}(z, \mathbf{x})$  and  $\mathbf{x}$  are the Eulerian and Lagrangian coordinates of the medium,  $\mathbf{v} \equiv \mathbf{v}_{\text{pec}}$  and  $\sigma_{\mathbf{v}}$  are the peculiar velocity and its variance, and  $\bar{g}'_z$  is the derivative with respect to the redshift  $z$ . The growth factor  $\bar{g} = \bar{g}(z)$  is normalized to unity at zero redshift ( $\bar{g}(0) = 1$ ), and at  $z > 1$ ,

$$\bar{g} \simeq \frac{1.3}{1+z} .$$

The Hubble function and the relation between the redshift and the peculiar velocity of matter at  $z > 1$  have the form

$$H \simeq 0.5 \cdot (1+z)^{3/2} H_0 , \quad (37)$$

$$\mathbf{v} \simeq 0.5 \cdot H_0 \sqrt{1+z} \bar{g} \mathbf{S} \simeq \frac{45}{\sqrt{1+z}} \left( \frac{\mathbf{S}}{\text{Mpc}} \right) \frac{\text{km}}{\text{s}} ,$$

To characterize small-scale motions of matter in a protohalo, we introduce the vector of the relative shift of medium points separated by a distance  $\mathbf{r}$  [see (30)]:

$$\mathbf{s} = \mathbf{s}(\mathbf{r}, \mathbf{x}) = \frac{\mathbf{S}(\mathbf{x} + \mathbf{r}) - \mathbf{S}(\mathbf{x})}{\sqrt{2} \sigma_{\mathbf{S}}} . \quad (38)$$

The vector  $\mathbf{s}$  describes the field of the normalized peculiar velocity of matter with the current radius vector  $\mathbf{r}$  referenced to the point  $\mathbf{x}$ . We are interested in the mean relative velocity and its variance during averaging over different ensembles (or points  $\mathbf{x}$ ) in different regions of the Universe.

The modulus of the radius vector  $r = |\mathbf{r}|$  is fixed in the interval of linear scales corresponding to inner regions of a gravitationally bound halo of size  $R$ :

$$r < R . \quad (39)$$

At  $R < \sigma_{\mathbf{S}}$ , these scales relate to the short-wavelength part of the spectrum  $P(k)$  (to the right of its maximum in Fig. 13),

$$k\sigma_{\mathbf{S}} \gg 1 : \quad P(k) \propto k^{-3} \ln^2(k\sigma_{\mathbf{S}}) .$$

Hence, we find the estimate for  $\sigma_r$  [see (25)]

$$\sigma_r^2 = \int_0^\infty P(k) W^2(kr) k^2 dk \propto \ln^3(2\sigma_{\mathbf{S}}/r) . \quad (40)$$

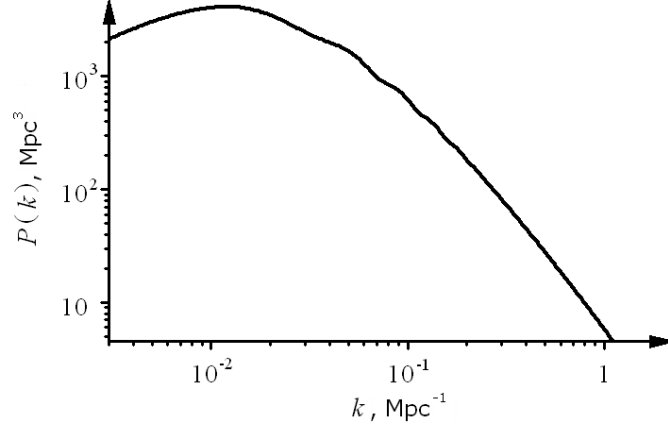


Figure 13: The power spectrum  $P(k)$  in the CSM,  $\sigma_{10} = 1$ .

Taking the power spectrum normalization  $\sigma_{10} \simeq 1$  into account, we can approximately calculate

$$1 \lesssim \sigma_R \sim \ln^{3/2}(2\sigma_{\mathbf{s}}/r) \quad \text{at} \quad R \lesssim 10 \text{ Mpc}.$$

At  $R > 10$  Mpc, a more accurate estimate for  $\sigma_R < 1$  should be used, taking the change in the spectral slope  $P(k)$  at scales of rich galaxy clusters into account.

Averaging over the entire Universe, we obtain the mean relative velocity and its variance:

$$\langle \mathbf{s} \rangle = 0, \quad (41)$$

$$\sigma_{\mathbf{s}}^2 \equiv \langle \mathbf{s}^2 \rangle = \sigma_{\mathbf{s}}^{-2} \int_0^\infty P(k) \left( 1 - \frac{\sin kr}{kr} \right) dk. \quad (42)$$

The random part of the velocity  $\sigma_{\mathbf{s}} = \sigma_{\mathbf{s}}(r)$  monotonically increases with increasing the scale (Fig. 14). At  $r < \sigma_{\mathbf{s}}$ , its growth is of a quasi-power form with a smoothly decreasing slope exponent, starting from unity:

$$\sigma_{\mathbf{s}} \simeq \frac{r\sigma_r}{\sqrt{6}\sigma_{\mathbf{s}}}.$$

The growth in the function  $\sigma_{\mathbf{s}}$  decreases at  $r \gtrsim \sigma_{\mathbf{s}}$  and saturates at  $r \gg \sigma_{\mathbf{s}}$ :  $\sigma_{\mathbf{s}} \rightarrow 1$ . At  $r = \sigma_{\mathbf{s}}$ ,  $\sigma_{\mathbf{s}} \simeq 1/2$ .

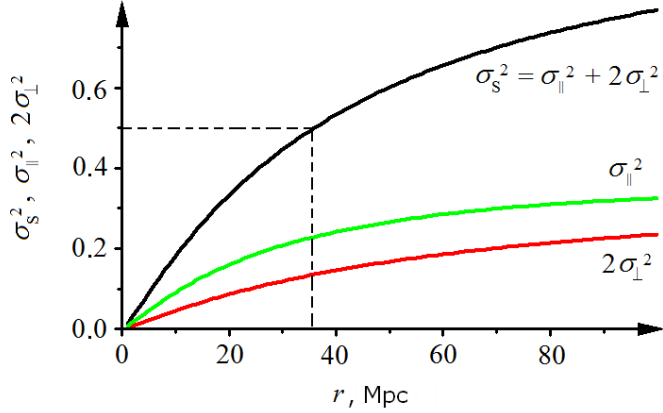


Figure 14: The variance of the relative velocity  $\sigma_{\mathbf{s}}^2(r)$  and its longitudinal  $\sigma_{\parallel}^2$  and transverse  $\sigma_{\perp}^2$  components (see [2]).

The correlation radius of function (42), at which  $\sigma_{\mathbf{s}}^2(r_{\mathbf{s}}) = 1/2$ , is  $r_{\mathbf{s}} \sim 36$  Mpc. We note that this is the mean correlation radius of the relative velocity of matter. The variance of vector (38) is anisotropic (different for the longitudinal and transverse components) and depends on the location of particles relative to the halo center  $\mathbf{r} = r\mathbf{e}$ :

$$c_{ij} \equiv \langle s_i s_j \rangle = \sigma_{\parallel}^2 e_i e_j + \sigma_{\perp}^2 p_{ij}, \quad (43)$$

$$\sigma_{\mathbf{s}}^2 = c_i^i = \sigma_{\parallel}^2 + 2\sigma_{\perp}^2, \quad (44)$$

where the tensor  $p_{ij} = \delta_{ij} - e_i e_j$  is the projector on the plane perpendicular to the vector  $\mathbf{e}$ ,

$$\sigma_{\parallel}^2 = \sigma_{\mathbf{s}}^{-2} \int_0^{\infty} P(k) \left[ \frac{1 + 2W(kr)}{3} - \frac{\sin kr}{kr} \right] dk,$$

$$\sigma_{\perp}^2 = \frac{1}{3} \sigma_{\mathbf{s}}^{-2} \int_0^{\infty} P(k) [1 - W(kr)] dk.$$

The correlation radii of the longitudinal and transverse variance are 20 Mpc ( $\sigma_{\parallel}^2 \simeq 1/6$ ) and 49 Mpc ( $\sigma_{\perp}^2 \simeq 1/6$ ).

Averaging over the ensemble of protohalos (see Appendix B) with a density contrast  $\nu_R$  [see (22)], we obtain the conditional expectations of small-scale velocities of matter in a protohalo:

$$\langle \mathbf{s} | \nu_R \rangle = \mathbf{c} \nu_R, \quad (45)$$

$$\sigma_{\mathbf{s}|\nu}^2 \equiv \langle \mathbf{s}^2 | \nu_R \rangle - \langle \mathbf{s} | \nu_R \rangle^2 = \sigma_{\mathbf{s}}^2 - \mathbf{c}^2, \quad (46)$$

where the cross-correlation coefficient has the form [see (39)]

$$\mathbf{c} \equiv \langle \mathbf{s} | \nu_R \rangle = -\frac{\mathbf{r}}{3\sqrt{2}\sigma_{\mathbf{S}}\sigma_R} \int_0^\infty P(k) W(kR) W(kr) k^2 dk \simeq -\frac{\mathbf{r}\sigma_R}{3\sqrt{2}\sigma_{\mathbf{S}}}.$$

Function (45) determines the universal velocity profile of a collapsing protohalo with the mass  $M_R$ . Conditional variance (46) describes dispersions of random deviations of the velocity from the mean value inside the protohalo:

$$\sigma_{\mathbf{s}|\nu}^2(r) = \sigma_{\mathbf{s}}^2 - \frac{1}{18} \left( \frac{r\sigma_R}{\sigma_{\mathbf{S}}} \right)^2. \quad (47)$$

## 11 A solution to the problem of galactic cusps

The suppression factor of peculiar motions of DM in a protohalo relative to the motions of matter in the Universe as a whole,

$$f(r|R) \equiv \frac{\sigma_{\mathbf{s}|\nu}^2}{\sigma_{\mathbf{s}}^2} \simeq 1 - \frac{1}{18} \left( \frac{r\sigma_R}{\sigma_{\mathbf{S}}\sigma_{\mathbf{S}}} \right)^2,$$

is shown in Fig. 15 for the galactic mass  $1.3 \cdot 10^{12} M_\odot$  ( $R = 2$  Mpc). For galaxies and groups of galaxies, the cross-correlation inside the protohalo is insignificant:

$$\sigma_{\mathbf{s}|\nu}^2(r) \simeq \frac{r^2}{6\sigma_{\mathbf{S}}^2} \left( \sigma_r^2 - \frac{1}{3}\sigma_R^2 \right) \simeq \sigma_{\mathbf{s}}^2, \quad (48)$$

and the variance of small-scale velocities of DM has the universal form, which is independent of the protohalo mass [see (36), (37)],

$$\sigma_{\mathbf{v}} \equiv \sigma_{\mathbf{v}} \sigma_{\mathbf{s}|\nu} \simeq \sigma_{\mathbf{v}} \sigma_{\mathbf{S}},$$

however, the value of the variance depends on the halo formation instant  $z$ .

By assuming that the coarse-grained entropy  $E(M)$  does not change in the protohalo contraction (see footnote 3 in Section 9), we obtain the mean profile of the background entropy mass function (8) in parametric representation [2, 41]:

$$\langle E_b \rangle = \frac{\sigma_{\mathbf{v}}^2}{3} \left( \frac{m_{\mathbf{p}}}{\rho(z)} \right)^{2/3} \propto \sigma_{\mathbf{s}}^2(r), \quad M = M_r \propto r^3. \quad (49)$$

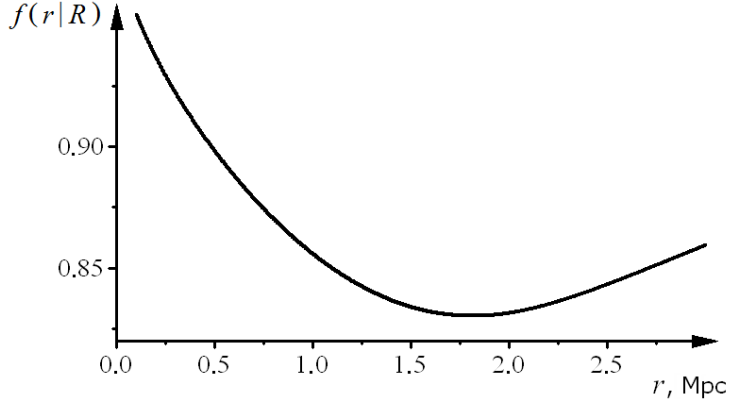


Figure 15: The suppression factor  $f(r|R)$  of peculiar velocities inside a halo with the mass  $M = 1.3 \times 10^{12} M_{\odot}$  (linear size  $R = 2$  Mpc) (see [2]).

Table 1: The power-law exponent of the background entropy function  $\beta_b$  for the central halo masses  $M \equiv 10^n M_{\odot} < M_R < 4 \cdot 10^{14} M_{\odot}$ .

$n$	12	10	8	6	4
$\beta_b$	0.34	0.45	0.50	0.53	0.56

Hence, we calculate the power-law slope exponent  $\beta_b$  depending on the index  $n$  of the central halo mass  $M \equiv 10^n M_{\odot} < M_R < M_{\mathbf{S}} \simeq 4 \cdot 10^{14} M_{\odot}$ :

$$\beta_b = \frac{d \ln \langle E_b \rangle}{d \ln M} = \frac{2}{3} - \frac{1}{\ln(2\sigma_{\mathbf{S}}/r)} \simeq \frac{2}{3} - \frac{1.3}{16 - n}, \quad (50)$$

The Table lists numerical values of  $\beta_b$  for different  $n$ . We see that in the halos of galaxies and groups of galaxies, the background entropy hampers the central cusp formation, because

$$\beta_b < 0.6 < \frac{5}{6}. \quad (51)$$

As  $R$  increases in the region  $R > \sigma_{\mathbf{S}}$  and the inner radius  $r < R$  increases proportionally (i.e., for large halos with  $M_R \geq 4 \cdot 10^{14} M_{\odot}$ ),<sup>4</sup> the cross-correlation

<sup>4</sup>We note that the radius of influence of dark matter  $r$  cannot be considered small,

$\langle \mathbf{s} \nu_R \rangle$  cannot be neglected anymore [see (47)], and small-scale motions of DM in the protohalo are suppressed. Therefore, the effect of the background entropy of DM inside rich galaxy clusters decreases.

Thus, DM cores are formed in the central region of halos of galaxies and galaxy groups. Following astronomical tradition, these DM cores can be appropriately called a spherical subsystem or ‘bulge’ of DM (in analogy with the baryonic bulge). By assuming that  $\alpha \sim 1$  in the region with maximum luminosity [see (29)], the Faber–Jackson relation must be valid for bulges, which is actually observed in elliptical galaxies. In disk and spiral galaxies, the bulge occupies a relatively small part of the halo, although its luminosity in the  $H_\alpha$  line can be significant, which apparently explains the Tully–Fisher relation.

In large spiral galaxies, the DM bulge is deformed due to baryonic inflow<sup>5</sup> however, its size is still quite large. For example, the bulge of our Galaxy occupies several kiloparsecs. As  $r$  increases, it transforms into a DM distribution with  $\rho \propto r^{-2}$  and an almost flat rotation curve, which in turn extends up to 10 kpc and, possibly, even further beyond the disk edge; further DM distribution can be probed by the motion of dwarf satellites.

On the other hand, numerical modeling shows that in gravitationally bound galaxy groups, the central bulge could be formed only in compact groups. There is a large class of smoothed galaxy groups that are only partially relaxed; such is the Local Group of galaxies. Its mass  $\sim 2 \cdot 10^{12} M_\odot$  is mainly due to the masses of two large spiral galaxies (the Milky Way and Andromeda Nebula) and also includes a small addition from masses of several

---

taking the cooling baryon flows and massive cD-galaxies in the cluster centers into account. For a similar reason, it makes no sense to consider central DM masses lower than that of black holes in galaxy centers. We should bear in mind in this connection that the characteristic scales of DM distributions are much larger than the sizes of central baryon condensations.

<sup>5</sup>It should be noted that during a slow baryonic inflow, the DM cusp (if it exists) would not be destroyed, but only enhanced. In this sense, it is asymptotically stable. The question is: what is the DM density in the halo center? This density, in particular, determines the possible flux of DM annihilation products (photons, positrons, antiprotons, etc.). Additional studies are needed to answer this question. Dwarf galaxies with low surface brightness appear to be ideal objects for studies of the central DM distribution (see Fig. 3), in which star formation is suppressed and the gas sustained in rotational equilibrium does not fall onto the halo center. Studies of spiral galaxies have not provided evidence of the existence of central cusps, either. Weak gravitational lensing plays an increasingly important role in reconstructing the DM surface density.

dozen dwarf galaxies.

When comparing theoretical predictions with observations, a wide dispersion in the background entropy distribution (and the corresponding inner density profiles) of relaxed halos, which is actually observed in galaxies (see Fig. 10) and follows from the CSM theory, should be taken into account. Indeed, for the initial Gaussian velocity perturbations, the probability distribution of the background entropy has the form

$$dp(f_b) = \frac{\exp(-f_b/2)}{\sqrt{2\pi f_b}} df_b, \quad (52)$$

where

$$f_b \equiv \frac{E_b}{\langle E_b \rangle} \simeq \frac{\mathbf{s}^2}{\sigma_s^2}.$$

We see that the halo background entropy has a wide distribution and its variances around mean value (49) are large:

$$\langle f_b \rangle = 1, \quad \langle f_b^2 \rangle = 3\langle f_b \rangle = 3.$$

These large values

$$\text{var } E_b > \langle E_b \rangle^2$$

imply significant deviations from the mean power-law slope exponents of the central density profiles in different galaxy halos, which is confirmed by observations.

The problem of galactic rotation curves is tightly connected with the inner structure of equilibrium halos, and we discuss it in Section 12.

## 12 Galactic rotation curves

In Section 5, we considered flat rotation curves of stellar and gas disks observed in many galaxies, which suggest an isothermal DM distribution inside halos in the range of radii and masses  $\lesssim 10$ . The corresponding power-law exponents of the density and entropy profiles in such systems [ $r > r_0$ ; see (11) and (24)] are

$$\alpha \simeq 2, \quad \beta \simeq \frac{4}{3}.$$

As noted in Section 6, similar distributions are generated in analytic models of the spherically symmetric or quasispherical collapse of gravitating dust

matter with a smooth initial density distribution, in which background small-scale perturbations are definitely absent. During nonlinear contraction of such a cloud, caustics (self-intersections) and multi-flow motions of matter arise in its central region, inducing a violent, collisionless relaxation. As a result of the gravitational redistribution of energy between spherical shells of matter, power-law density and entropy profiles are formed in the central parts of the halo, with the exponents

$$1.6 < \alpha_g < 2, \quad 1 < \beta_g < 1.3. \quad (53)$$

It follows from (53) that the violent relaxation leads to the entropy distribution implying the formation of a cusp. However, these exponents are related to rather large radii. In the central halo, generated entropy (53) cannot compete with the background one and turns out to be negligibly small (see the Table). Therefore, the background entropy effect constrains the central density and hinders the formation of cusp-like halo profiles.

The same conclusion is valid for the numerical experiment modeling of the most complex stages of halo formation that cannot be treated analytically. Violent relaxation, in which radial trajectories play the dominant role, is not the only and, possibly, the main relaxation process of collisionless systems that decoupled from the Friedman flow during cosmological expansion. An important role here is played by anisotropic collapse and the effects of merger of clumps with different masses that were formed before the central massive part and simultaneously with it. All these processes, which are actually observed in nonlinearly relaxing gravitationally bound systems at high redshifts, are called hierarchical clustering. They include the tidal binary (and also triple, etc.) interaction of clumps of matter captured in the common gravitational field and their scattering and merging into more massive objects with the subsequent repetition of the entire cycle.

The development of numerical modeling techniques for a large number of gravitationally interacting bodies has led to the notion of the universal halo density NFW profile, which appears after averaging the density profiles in several hundred clumps of different masses and sizes formed during the merger. The initial particle distribution in the N-body problem is taken to be close to cosmological conditions, but because the number N is finite, the dynamical range of model scales is restricted. As noted in Section 6, the NFW profile asymptotically approaches a cusp-like power law with the

exponents

$$\alpha_g = 1 \quad , \quad \beta_g = \frac{5}{6} \quad .$$

In numerical modeling of the  $N$ -body problem, the background entropy of small-scale perturbations is apparently underestimated due to the restricted spatial resolution of this method. Hopefully, as the power of numerical methods increases, the background entropy effects can be properly taken into account.

Already much evidence has appeared showing that with increasing  $N$ , the exponent  $\alpha$  decreases below unity; however, these are single examples and no statistics can be applied. Due to the small-scale cut-off of the model power spectrum, the initial entropy effect is suppressed in comparison with the analytic estimates shown in the Table.

Of course, the background entropy effect on the internal halo structure and the formation of the central core with finite pressure and DM density should be confirmed by numerical experiment. Nevertheless, today we can already verify the CSM predictions by measuring velocities of gas and stars in galaxies and galaxy clusters.

Figure 3 demonstrates galactic rotation curves that cannot be described by formula (19) but are well approximated by a smoother profile in (18). Such examples are typical for galaxies (see, e.g., [64]). In the central region with  $r < r_s$ , the fit constructed using the observational points is similar to the isothermal sphere approximation [see (16) and (17)]; but at large radii, the density decrease is inversely proportional to  $r^3$  and circular velocities slowly decrease. The circular velocity reaches a maximum at the point of the local density profile with the exponent  $\alpha = 2$ .

Simulated NFW profiles meet with another problem: they do not reproduce flat galactic rotation curves in the observed range of scales. Nevertheless, numerical profiles provide a good approximation of the mass distribution in galaxy clusters (see Fig. 4, 5).

## 13 Effect of the background entropy

To understand the physical meaning and variety of the observed rotation curves, the initial background entropy of DM in nonlinear halos should be taken into account.

To clarify the physics of this effect, we consider the simplest model of the joint entropy mass function in the form

$$E(M) = \sqrt{E_b^2 + E_g^2}, \quad f_b = \frac{E_b}{E}, \quad (54)$$

where the parameter  $f_b \in (0, 1)$  expresses the relative contribution of the background entropy at a fixed inner halo radius corresponding to the circular velocity maximum or the local density profile slope  $\alpha = 2$ . The functions  $E_{b,g}(M)$  have a power-law form with the corresponding slope exponents in the ranges

$$\beta_b \in \left(\frac{1}{3}, \frac{2}{3}\right), \quad \beta_g \in \left(\frac{5}{6}, \frac{4}{3}\right). \quad (55)$$

We now can calculate the rotation curves of particles in equilibrium DM halos analytically and compare them with observations and numerical model calculations. The results are presented in Fig. 16. The rotation velocities  $v_{\text{rot}} = v(r)$  as functions of the inner radius  $r$  are obtained for models of hierarchical ( $\beta_g = 5/6$ , Fig. 16a) and violent ( $\beta_g = 4/3$ , Fig. 16b) relaxations for two limit values of  $f_b$ ,  $f_b \ll 1$  and  $f_b \sim 1$ , and three values of the background entropy indices. Velocities and radii are normalized to the corresponding maximum values of the velocity and the radius  $r_{-2}$  at which it is attained:  $v_{\text{max}} \equiv v(r_{-2}) \geq v(r)$ . We see from this figure that for halos with  $\beta_b < 0.5$  and any parameters  $\beta_g$  and  $f_b$  in the chosen intervals, the induced rotation curves fully cover the range between the NFW and Burkert approximations. For  $f_b \ll 1$ , the curves shift to the NFW region, while as  $f_b$  increases, they become similar to the Burkert profiles.

It follows that the observed rotation curves are successfully reproduced by simple models (54) with the corresponding fitting parameters  $f_b$  and  $\beta_b$ . Distributions of the background (52) and generated (55) entropies in the halo allow explaining the required diversity of the observed galactic rotation curves. As the exponent  $\beta_b$  increases, the rotation curves concentrate closer to the NFW profiles.

The examples considered here prove the following.

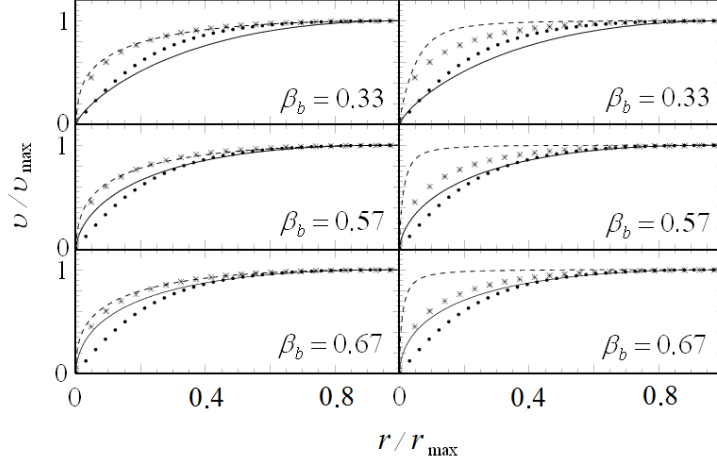


Figure 16: Normalized rotation curves  $v(r)$  for models of (a) hierarchical ( $\beta_g = 5/6$ ) and (b) violent ( $\beta_g = 4/3$ ) relaxation at  $f_b \ll 1$  (the dashed curve) and  $f_b \simeq 1$  (the solid curve) (see [41]). The NFW and Burkert approximations are respectively shown by X's and the dotted line.

- The background entropy prevents the formation of central DM cusps in halos in the mass range  $10^8 - 10^{14} M_\odot$ . For heavier and lighter halos, the background entropy effect is attenuated.
- Taking the effect of the background entropy on the density distribution inside a halo into account allows reproducing the rotation curves in a wide range of scales and can solve the problem of DM cusps in the CSM framework.

To conclude, we note that the models considered here are based on simple assumptions of the DM particle distribution in the halo and neglect the contribution of baryonic matter. The full problem of the evolution of galactic density profiles, including DM and baryons and accounting for the effect of different dissipative processes on the angular momentum transfer from the central parts of galaxies, is undoubtedly very complicated and requires further studies, both analytic and numerical.

## 14 Conclusion

The entropy method of description of virialized DM systems considered here allows an analytic treatment of these complex nonlinear structures. It enables connecting the inner DM density profiles with characteristics of both the initial small-scale field of density perturbations and the nonlinear large-scale relaxation of gravitationally contracted matter. We conclude that cosmological random motions of matter ‘warm up’ DM particles in the collapsing protohalos. We have shown that taking this effect into account

- leads to suppression of cusp-like density profiles in the forming halo and to the formation of DM cores in galaxies;
- allows explaining the diversity of galactic rotation curves, both observed and obtained in numerical simulations;
- helps to solve the problem of the inner structure of equilibrium DM halos in the CSM framework.

The obtained analytic results should be confirmed by numerical  $N$ -body experiments, which can be done in the future with improved spatial resolution of the central halo parts.

The authors thank S V Pilipenko for the fruitful discussions.

This work was supported by the Russian Foundation for Basic Research grants 11-02-12168-ofi-m-2011 and 11-02-00244, and by the FCP program ‘Scientific and Scientific–Pedagogical Specialists of Innovative Russia’ for 2009–2013 (state contracts P1336 and 16.740.11.0460).

## 15 Appendices

### Appendix A. Correlation functions of the initial perturbations

Fourier harmonics of the linear density perturbation field are  $\delta$ -correlated:

$$\delta(\mathbf{x}) = (2\pi)^{-3/2} \int \delta_{\mathbf{k}} e^{i\mathbf{k}\mathbf{x}} d\mathbf{k}, \quad \langle \delta_{\mathbf{k}} \delta_{\mathbf{k}'}^* \rangle = 2\pi^2 P(k) \delta^{(3)}(\mathbf{k} - \mathbf{k}'),$$

where the averaging  $\langle \dots \rangle$  is done over all realizations of the random Gaussian field,  $\delta^{(3)}(\mathbf{k})$  is the three-dimensional Dirac  $\delta$ -function, and  $P = P(k)$  is the power spectrum.

Using this decomposition, we can construct any correlators of the cosmological perturbation field, for example

$$\begin{aligned}\langle \delta(\mathbf{x} + \mathbf{r}) \delta(\mathbf{x}) \rangle &= \int_0^\infty P(k) \frac{\sin kr}{kr} k^2 dk, \\ \langle \mathbf{S}(\mathbf{x} + \mathbf{r}) \delta(\mathbf{x}) \rangle &= -\frac{\mathbf{r}}{3} \int_0^\infty P(k) W(kr) k^2 dk, \\ \langle S_j(\mathbf{x} + \mathbf{r}) S_k(\mathbf{x}) \rangle &= e_j e_k \int_0^\infty P(k) \left[ \frac{\sin kr}{kr} - \frac{2}{3} W(kr) \right] dk + \\ &\quad + \frac{1}{3} p_{jk} \int_0^\infty P(k) W(kr) dk\end{aligned}$$

where  $\mathbf{e} = e_j = r_j/r$  is the unit vector in the direction  $\mathbf{r}$ ,  $p_{jk}$  is the projection tensor [see (43)],  $\delta = -\text{div } \mathbf{S}$ , and  $\mathbf{S}$  is the shift vector of matter elements [see (30)-(37)],

$$\mathbf{S} = S_j = i(2\pi)^{-3/2} \int \frac{k_j}{k^2} \delta_{\mathbf{k}} e^{i\mathbf{k}\mathbf{x}} d\mathbf{k}$$

We can represent smoothed fields similarly, for example,

$$\begin{aligned}\delta_R &= (2\pi)^{-3/2} \int \delta_{\mathbf{k}} W(kR) e^{i\mathbf{k}\mathbf{x}} d\mathbf{k}, \\ \langle \mathbf{S}(\mathbf{x} + \mathbf{r}) \delta_R(\mathbf{x}) \rangle &= -\frac{\mathbf{r}}{3} \int_0^\infty P(k) W(kR) W(kr) k^2 dk,\end{aligned}$$

etc.

## Appendix B. Conditional probability distribution

To obtain the conditional probability  $p(\mathbf{s}|\nu_R)$  of  $\mathbf{s}$  for a given value of  $\nu_R$ , we consider the Gaussian distribution of two variables  $x_A = (\mathbf{s}, \nu_R)$  with the index  $A$  ranging over the values  $i, R$ :

$$p(\mathbf{s}, \nu_R) = \frac{\exp(-\kappa^2/2)}{(2\pi)^2 \sqrt{C}}, \quad \kappa^2 = c^{AB} x_A x_B,$$

where  $c^{AB}$  is the inverse matrix to the matrix [see (43), (45)]

$$c_{AB} = \langle x_A x_B \rangle = \begin{pmatrix} c_{ij} & \mathbf{c} \\ \mathbf{c} & 1 \end{pmatrix},$$

$$C \equiv \det(c_{AB}) = \bar{\sigma}_{\parallel}^2 \sigma_{\perp}^4, \quad \bar{\sigma}_{\parallel}^2 = \sigma_{\parallel}^2 - \mathbf{c}^2.$$

After simple transformations, we obtain

$$\kappa^2 = \bar{\kappa}^2 + \nu_R^2, \quad \bar{\kappa}^2 = \bar{c}^{ij} \bar{s}_i \bar{s}_j, \quad \bar{\mathbf{s}} = \mathbf{s} - \mathbf{c} \nu_R,$$

where  $\bar{c}^{ij}$  is the matrix inverse to

$$\bar{c}_{ij} \equiv \langle \bar{s}_i \bar{s}_j | \nu_R \rangle = \bar{\sigma}_{\parallel}^2 e_i e_j + \sigma_{\perp}^2 p_{ij}.$$

Hence, we find the conditional probability distribution of the vector  $\mathbf{s}$  and the variance of velocities inside a halo with the density contrast  $\nu_R$ :

$$p(\mathbf{s} | \nu_R) = \frac{p(\mathbf{s}, \nu_R)}{p(\nu_R)} = \frac{\exp(-\bar{\kappa}^2/2)}{(2\pi)^{3/2} \bar{\sigma}_{\parallel} \sigma_{\perp}^2},$$

$$\sigma_{\mathbf{s}|\nu}^2 \equiv \langle \bar{\mathbf{s}}^2 | \nu_R \rangle = \sigma_{\mathbf{s}}^2 - \mathbf{c}^2.$$

## References

- [1] Lukash V N, Mikheeva E V, Malinovsky A M *Usp. Fiz. Nauk* **181** 1017 (2011) [*Phys. Usp.* **54** 983 (2011)]
- [2] Lukash V N, Mikheeva E V *Fizicheskaya Kosmologiya (Physical Cosmology)* (Moscow: FIZMATLIT, 2010)
- [3] Navarro J F, Frenk C S, White S D M *Mon. Not. R. Astron. Soc.* **275** 720 (1995)
- [4] Navarro J F, Frenk C S, White S D M *Astrophys. J.* **462** 563 (1996)
- [5] Navarro J F, Frenk C S, White S D M *Astrophys. J.* **490** 493 (1997)
- [6] Pointecouteau E, Arnaud M, Pratt G W *Astron. Astrophys.* **435** 1 (2005)
- [7] Tasitsiomi A et al. *Astrophys. J.* **607** 125 (2004)
- [8] Hayashi E et al. *Mon. Not. R. Astron. Soc.* **355** 794 (2004)
- [9] Peebles P J E *Astrophys. J.* **147** 859 (1967)

- [10] Peebles P J E *The Large-Scale Structure of the Universe* (Princeton, N.J.: Princeton Univ. Press, 1980)
- [11] Press W H, Schechter P *Astrophys. J.* **187** 425 (1974)
- [12] Peacock J A, Heavens A F *Mon. Not. R. Astron. Soc.* **243** 133 (1990)
- [13] Bower R *Mon. Not. R. Astron. Soc.* **248** 332 (1991)
- [14] Bond J R et al. *Astrophys. J.* **379** 440 (1991)
- [15] Manrique A, Salvador-Solé E *Astrophys. J.* **453** 6 (1995)
- [16] Manrique A, Salvador-Solé E *Astrophys. J.* **467** 504 (1996)
- [17] Bond J R, Myers S T *Astrophys. J. Suppl.* **103** 63 (1996); *Astrophys. J. Suppl.* **103** 1 (1996)
- [18] Sheth R K, Tormen G *Mon. Not. R. Astron. Soc.* **308** 119 (1999)
- [19] Raig A, González-Casado G, Salvador-Solé E *Mon. Not. R. Astron. Soc.* **327** 939 (2001)
- [20] Manrique A et al. *Astrophys. J.* **593** 26 (2003)
- [21] White S D M, Zaritsky D *Astrophys. J.* **394** 1 (1992)
- [22] Sikivie P, Tkachev I I, Wang Y *Phys. Rev. D* **56** 1863 (1997)
- [23] Nusser A *Mon. Not. R. Astron. Soc.* **325** 1397 (2001)
- [24] Arkhipova N A et al. *Grav. Cosmology Suppl.* **8** 66 (2002)
- [25] Arkhipova N A et al. *Astron. Zh.* **84** 874 (2007) [*Astron. Rep.* **51** 787 (2007)]
- [26] Williams L L R, Babul A, Dalcanton J J *Astrophys. J.* **604** 18 (2004)
- [27] Demiański M, Doroshkevich A G *Astron. Astrophys.* **422** 423 (2004)
- [28] Fillmore J A, Goldreich P *Astrophys. J.* **281** 1 (1984)
- [29] Gurevich A V, Zybin K P *Zh. Eksp. Teor. Fiz.* **94** 3 (1988) [*Sov. Phys. JETP* **67** 1 (1988)]

- [30] Gurevich A V, Zybin K P *Usp. Fiz. Nauk* **165** 723 (1995) [*Phys. Usp.* **38** 687 (1995)]
- [31] Avila-Reese V, Firmani C, Hernández X *Astrophys. J.* **505** 37 (1998)
- [32] Tormen G, Bouchet F R, White S D M *Mon. Not. R. Astron. Soc.* **286** 865 (1997)
- [33] Syer D, White S D M *Mon. Not. R. Astron. Soc.* **293** 337 (1998)
- [34] Nusser A, Sheth R K *Mon. Not. R. Astron. Soc.* **303** 685 (1999)
- [35] Dekel A et al. *Astrophys. J.* **588** 680 (2003)
- [36] Gao L et al. *Astrophys. J.* **614** 17 (2004)
- [37] Voglis N, Hiotelis N, Harsoula M *Astrophys. Space Sci.* **266** 213 (1995)
- [38] Zaroubi S, Naim A, Hoffman Y *Astrophys. J.* **457** 50 (1996)
- [39] Avila-Reese V et al. *Astrophys. J.* **559** 516 (2001)
- [40] Demiański M, Doroshkevich A G *Mon. Not. R. Astron. Soc.* **306** 779 (1999)
- [41] Mikheeva E, Doroshkevich A, Lukash V *Nuovo Cimento B* **122** 1393 (2007)
- [42] Taylor J E, Navarro J F *Astrophys. J.* **563** 483 (2001)
- [43] Ostriker J P, Bode P, Babul A *Astrophys. J.* **634** 964 (2001); arXiv:astro-ph/0504334v2
- [44] Kravtsov A, *Advances in Astronomy* 281913 (2010); arXiv:0906.3295v1
- [45] Catinella B, Giovanelli R, Haynes M P *Astrophys. J.* **640** 751 (2006)
- [46] Vikhlinin A et al. *Astrophys. J.* **692** 1060 (2009)
- [47] Freese K, arXiv:0812.4005v1
- [48] Marchesini D et al. *Astrophys. J.* **575** 801 (2002)
- [49] Burkert A *Astrophys. J.* **447** L25 (1995)

- [50] Moore B *Nature* **370** 629 (1994)
- [51] Moore B et al. *Astrophys. J.* **499** L5 (1998)
- [52] Diemand J, Moore B, Stadel J *Nature* **433** 389 (2005)
- [53] Pilipenko S V, Doroshkevich A G, Gottlöber S *Astron. Zh.* **86** 1050 (2009) [*Astron. Rep.* **53** 976 (2009)]
- [54] Navarro J F, arXiv:astro-ph/0311361v1
- [55] Gentile G, Tonini C, Salucci P *Astron. Astrophys.* **467** 925 (2007); arXiv:astro-ph/0701550v1
- [56] Karachentsev I D et al. *Mon. Not. R. Astron. Soc.* **393** 1265 (2009)
- [57] Dalcanton J et al. *Astrophys. J. Suppl.* **183** 67 (2009)
- [58] Springel V et al. *Mon. Not. R. Astron. Soc.* **391** 1685 (2008)
- [59] Kopolov S et al. *Astrophys. J.* **686** 279 (2008)
- [60] Macció A V et al. *Mon. Not. R. Astron. Soc.* **402** 1995 (2010)
- [61] de Blok W J G et al. *Astrophys. J.* **552** L23 (2001)
- [62] Faber S M, Jackson R E *Astrophys. J.* **204** 668 (1976)
- [63] Tully R B, Fisher J R *Astron. Astrophys.* **54** 661 (1977)
- [64] Evans N W, An J, Walker M G *Mon. Not. R. Astron. Soc.* **393** L50 (2009)